nature astronomy

LETTERS

https://doi.org/10.1038/s41550-018-0551-8

# The inside-out planetary nebula around a born-again star

Martín A. Guerrero[1]*, Xuan Fang[2], Marcelo M. Miller Bertolami[3,4], Gerardo Ramos-Larios[5], Helge Todt[6], Alexandre Alarie[7], Laurence Sabin[7], Luis F. Miranda[1], Christophe Morisset[7], Carolina Kehrig[1] and Saúl A. Zavala[8]

**Planetary nebulae are ionized clouds of gas formed by the hydrogen-rich envelopes of low- and intermediate-mass stars ejected at late evolutionary stages. The strong UV flux from their central stars causes a highly stratified ionization structure, with species of higher ionization potential closer to the star. Here, we report on the exceptional case of HuBi 1, a double-shell planetary nebula whose inner shell presents emission from low-ionization species close to the star and emission from high-ionization species farther away. Spectral analysis demonstrates that the inner shell of HuBi 1 is excited by shocks, whereas its outer shell is recombining. The anomalous excitation of these shells can be traced to its low-temperature [WC10] central star whose optical brightness has declined continuously by 10 magnitudes in a period of 46 years. Evolutionary models reveal that this star is the descendant of a low-mass star (≃1.1 $M_{\odot}$) that has experienced a 'born-again' event[1] whose ejecta shock-excite the inner shell. HuBi 1 represents the missing link in the formation of metal-rich central stars of planetary nebulae from low-mass progenitors, offering unique insight regarding the future evolution of the born-again Sakurai's object[2]. Coming from a solar-mass progenitor, HuBi 1 represents a potential end-state for our Sun.**

Planetary nebulae (PNe) are a short-lived ≈20,000 yr period in the transition of low- and intermediate-mass stars ($M_{\rm initial}$ = 0.8–8.0 $M_{\odot}$) from the asymptotic giant branch (AGB) phase towards the white-dwarf (WD) phase. The ionization structure of PNe, governed by the distance of the nebular material to the central star of the PN (CSPN), is well known to display an 'onion-like' structure with higher ionization species such as $He^{++}$ and $O^{++}$ close to the central star, lower ionization species such as $N^{+}$ and $O^{+}$ in the outer region, and neutral and molecular species such as $O^{0}$ and $H_2$ in the outermost photo-dissociation region.

Whereas this is the general rule, we have discovered an exceptional case in HuBi 1 (ref.[3]) (PN G012.2+04.9, also known as PM 1-188). Originally reported to have a faint bipolar outer shell and an unresolved bright inner shell[4], our sub-arcsec resolution images (Fig. 1a) and spatial profiles of selected emission lines (Fig. 1b–d) extracted from sub-arcsec long-slit spectroscopic observations refine this description, while unveiling a puzzling fact: the outer shell of HuBi 1, a barrel-like structure with faint polar protrusions slightly inclined to the line of sight (see Methods), surrounds a [N II]-bright inner shell (Fig. 1b). The low-excitation inner shell of HuBi 1 is unusual among PNe, but its ionization structure is even more peculiar (Fig. 1c,d). The spatial profile of the [O II] $\lambda$3727 emission line fills the inner shell cavity whose rim is defined by the [N II] $\lambda$6548 and [O III] $\lambda$5007 emission lines. This is exactly opposite to typical photoionized nebulae, where the [N II] and [O II] spatial profiles are generally coincident with each other and the [O III] profile peaks inside, given the very similar ionization potentials required for $O^{+}$ and $N^{+}$ and the higher ionization potential for $O^{++}$. More surprisingly, perhaps, the spatial profile of the He II $\lambda$4686 line peaks outside those of [N II] and [O III], although the ionization potential for $He^{++}$ is higher than for $N^{+}$ and $O^{++}$. The ionization structure of the inner shell of HuBi 1 is inverted with respect to that of photoionized nebulae. In this sense, HuBi 1 is inside-out.

The origin of the inverted ionization structure of the inner shell of HuBi 1 must be at its CSPN, IRAS 17514-1555 (hereafter IRAS 17514). This star is of [WR]-type, that is, its spectrum shows relatively broad emission lines similar to those of massive Wolf–Rayet (WR) stars[5] that indicate H-deficient strong stellar winds. The spectrum of IRAS 17514, which reveals a wealth of C II and C III emission lines[4] arising from a C-rich stellar wind, has been assigned a spectral type of [WC10] (ref. [6]). Our analysis of mid-1990s spectroscopic observations of IRAS 17514 using state-of-the-art non-LTE (local thermodynamic equilibrium) models (see Methods) confirms its low terminal wind velocity $v_{\infty} \approx 360\,{\rm km\,s^{-1}}$, low surface temperature $T_{\star} \approx 38,000\,{\rm K}$, and high C and O abundances[7]. The number of $He^{+}$ ionizing photons suggested by this non-LTE stellar model, $\log Q({\rm He\,II}) < 34$, is much lower than that derived for the nebula, $\log Q({\rm He\,II}) > 43.8$ (see Methods). Not only is the spatial distribution of the He II emission in HuBi 1 unexpected for a photoionized nebula, but its detection is puzzling because the CSPN is not hot enough to photoionize $He^{+}$.

The actual state of affairs is more complex yet. A revision of long-term optical photometry and spectroscopy of IRAS 17514 (see Methods) reveals it has faded continuously over time (Fig. 2). Back to March 1989, the star had a $V$-band magnitude of 14.6, which faded to 19.8 in June 2014, and was above a detection limit ≥22.7 in May 2017. Using archival USNO B-1 data obtained on January 1971, we found a decline in the $B$ and $R$ bands by nearly 10 magnitudes, implying a decrease in optical brightness ≅10,000 times in 46 years. The spectral changes in IRAS 17514 during the period from 1996 to

[1]Instituto de Astrofísica de Andalucía, IAA-CSIC, Granada, Spain. [2]Laboratory for Space Research & Department of Physics, Faculty of Science, The University of Hong Kong, Hong Kong, People's Republic of China. [3]Instituto de Astrofísica de La Plata, UNLP-CONICET, La Plata, Argentina. [4]Facultad de Ciencias Astronómicas y Geofísicas, UNLP, La Plata, Argentina. [5]Instituto de Astronomía y Meteorología, Departamento de Física CUCEI, Universidad de Guadalajara, Guadalajara, Jalisco, Mexico. [6]Institute of Physics and Astronomy, University of Potsdam, Potsdam, Germany. [7]Instituto de Astronomía, Universidad Nacional Autónoma de México, Ensenada, Baja California, Mexico. [8]Tecnológico Nacional de México/I.T. Ensenada, Departamento de Ciencias Básicas, Ensenada, Baja California, Mexico. *e-mail: mar@iaa.es

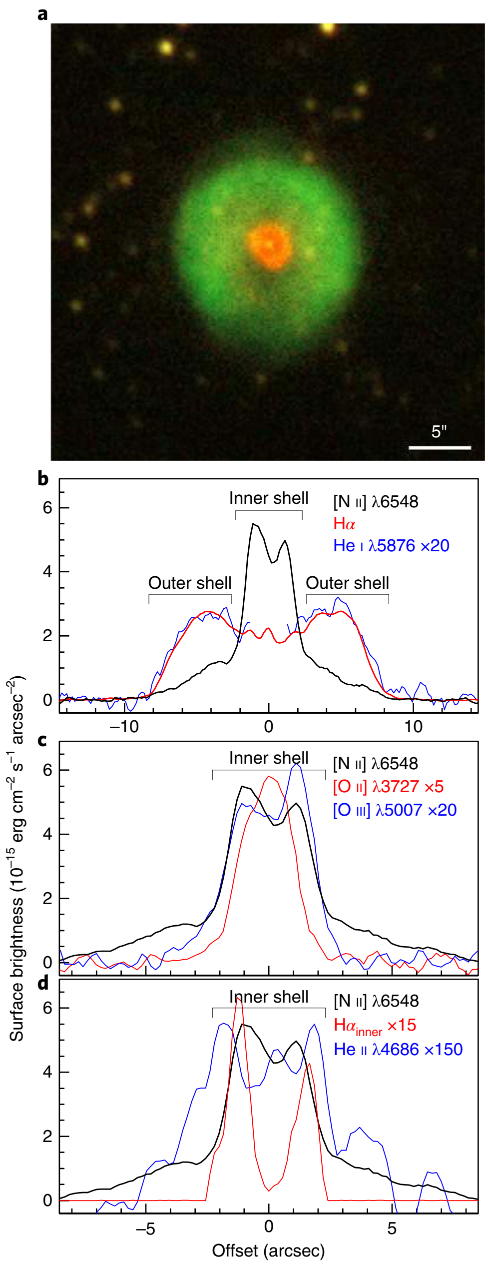


**Fig. 1 | Colour composite picture and spatial profiles of selected lines of HuBi 1. a**, NOT ALFOSC [N II] λ6584 (red) and Hα λ6563 (green) colour composite picture of HuBi 1. Hα emission dominates the 18.4″ × 19.2″ outer shell, whereas the ≃4″ inner shell is brighter in [N II]. **b**–**d**, Continuum-subtracted spatial profiles of nebular emission lines (see Methods) along the east–west direction of HuBi 1 across its central star for the outer (**b**) and inner shells (**c**,**d**). The Hα spatial profile of the inner shell in **d** is computed by subtracting a model for the total Hα emission of the outer shell from the total emission profile in **b** (see Methods). The extent of the inner and outer shells, as used to extract one-dimensional spectra, are marked.

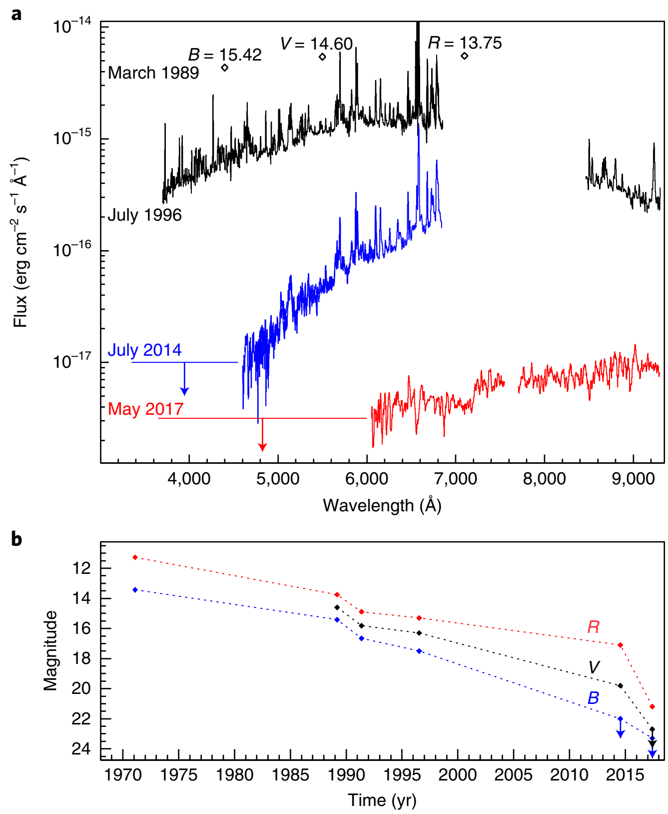


**Fig. 2 | Long-term spectro-photometric evolution of IRAS 17514, the central star of HuBi 1. a**, Optical spectra obtained at different epochs between July 1996 and May 2017. The March 1989 *BVR* magnitudes from the paper that first reported HuBi 1 (ref. [3]) are included for reference. The horizontal lines and down-pointing arrows indicate detection upper limits. **b**, Time evolution of the *BVR* magnitudes of IRAS 17514 as derived from photometric or spectroscopic measurements. Down-pointing arrows indicate detection limits.

2014 are mainly restricted to its stellar continuum, as the profiles and equivalent widths of the spectral lines remained unchanged. Since spectral lines are very sensitive to $T_\star$, a change of $T_\star > 2{,}000$ K can be discarded. Such small variation in $T_\star$ would imply a tiny change in the optical flux, which depends almost linearly on $T_\star$ given that the optical region of a CSPN spectrum can be approximated with the Rayleigh–Jeans law. Rather, the decline in time of the optical flux of IRAS 17514 is associated with a correlated increase in obscuration.

At the present time, IRAS 17514 cannot even provide the ionizing flux required to keep hydrogen ionized in HuBi 1, which is estimated to be $\log Q(\mathrm{H\,I}) = 45.7$. With such a rapidly fading CSPN, the nebula is expected to exhibit unusual spectral properties. Indeed, the spectra of the inner and outer shells have their own share of peculiarities (see Methods). The outer shell is dominated by H I and He I recombination lines, with much fainter emission of forbidden lines, which is reminiscent of recombining haloes in PNe[8]. MAPPINGS photoionization models following the time evolution of a low-density photoionized PN after the ionizing UV flux from its CSPN ceases show that its cooling timescale is only a few decades, whereas its recombination timescale is much longer, several thousand years (see Methods). As for the inner shell, the brightest emission lines in its spectrum are those of [N II], with the notable detection of the He II line at 4,686 Å. The inverted ionization structure and spectrum of this shell are typical of shocks propagating through an ionized medium[9]. Indeed, where the CLOUDY photoionization models using the best-fit non-LTE stellar atmosphere model of IRAS 17514 fail to reproduce those, MAPPINGS models including shock excitation are successful for shock velocities ≳ 70 km s$^{-1}$ (see Methods). As the shock travels outwards through the ionized outer shell of HuBi 1, He II emission arises at the location of the shock, while the [O II], [O III] and [N II] emissions originate at the post-shock cooling region.

Therefore, HuBi 1 is a fossil nebula surrounding a shock-excited inner shell. Its CSPN, IRAS 17514, has recently started ejecting large

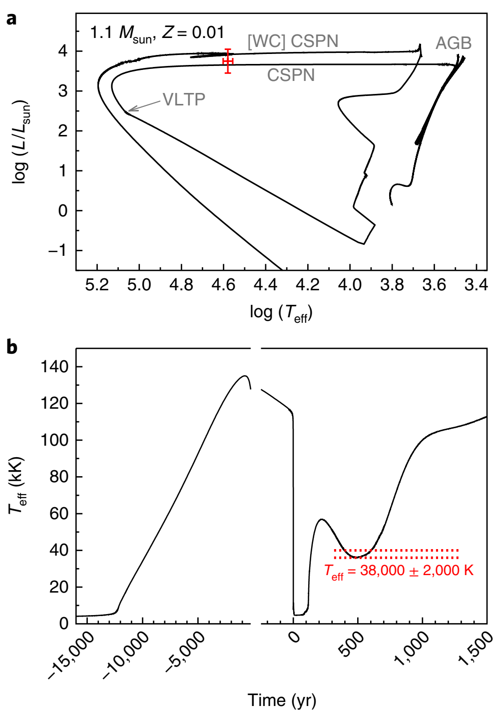


**Fig. 3 | Evolutionary sequence of a PN progenitor with initial mass 1.1 $M_\odot$ that experiences a VLTP.** **a**, Evolutionary track in the HR diagram. The post-AGB star has a mass of 0.551 $M_\odot$. The red cross indicates the current location (with uncertainties) of HuBi 1 CSPN. **b**, Post-AGB time evolution of $T_{eff}$. The time origin in this plot is set at the moment of the VLTP event, with different timescales being used before and after it. Note that the star departed from the AGB phase ≈12,000 yr before the occurrence of the VLTP, as marked by the initial increase of $T_{eff}$ in this plot. The red-dotted lines mark the uncertainty in the temperature of the central star of HuBi 1, which is constrained by the ionization balance of the carbon and silicon ions as derived from the observed relative line strengths of C II, C III and C IV lines, and Si III and Si IV lines (see Methods for further details).

amounts of C-rich material at speeds faster than the nebular expansion. The expansion of this ejecta shock-excites the inner shell and, as it streams away, it cools down to conditions optimal for condensation of dust grains[10]. The increasing optical depth of the dusty circumstellar cocoon shields the UV photons from the CSPN, so that the outer nebula cools down and has started recombining.

Obviously, this is not the classical behaviour for a CSPN. Dramatic drops in luminosity have been observed in slow novae[11] and R CrB stars[12], but the spectral properties and variation timescale of these sources differ from those of IRAS 17514. The C-rich dense stellar winds of (truly massive) WC stars provide suitable sites for dust production[13], either in episodic WC dust makers associated with eccentric binary systems with colliding winds (CWB) or persistent WC dust makers (WCd). We note that the photometric behaviour of WCd stars, with short (days to weeks) episodes of diminished brightness up to a few magnitudes[14], does not fit that of HuBi 1.

The key to understanding HuBi 1 is the [WC] nature of its CSPN. [WC]-type central stars account for a non-negligible fraction (~15%) of CSPNe[15], but their origin is still debated. It has been proposed that they form through a thermal pulse, either at the end of the AGB (a final thermal pulse, FTP), during the post-AGB evolution of the CSPN when H-burning is still active (a late thermal pulse, LTP[16]), or early in the cooling phase of the WD evolution (a very late thermal pulse, VLTP[17]). These different channels result in different size and density of the PN, as well as distinct chemical composition of the CSPN. An FTP will result in a dense and dusty nebula with bright IR emission around the [WC] star, which has been suggested for the IR-[WC] class[18]. The old kinematical age and low density of the outer shell of HuBi 1 (≈9,000 years and ≈200 cm$^{-3}$, respectively, see Methods) rather favour a VLTP. Born-again events such as V605 Aql, V4334 Sgr (also known as the Sakurai's object) and FG Sge imply notable stellar temperature variations in short (a few years[1,2]) timescales and even faster drops in luminosity, within days or weeks; but these are not observed in IRAS 17514. Ad hoc late stellar evolution models following VLTP events of low-mass progenitors reveal loops in the Hertzsprung–Russell (HR) diagram resulting in extended phases of stalled $T_{eff}$ (see Methods). The observed properties of HuBi 1 (kinematical age) and its CSPN (luminosity, surface temperature in the 1996–2014 period and stellar wind abundances) can be reproduced with a VLTP in a 1.1 $M_\odot$ progenitor (Fig. 3).

IRAS 17514 is caught in a brief but key episode in the evolution of a [WC] star and the nebula around it, which can be described by a low-mass born-again event. The ejecta associated with this VLTP is propagating a shock through the surrounding outer shell of HuBi 1, resulting in an inner shell with an inverted ionization structure unequalled among PNe, while its kinetic energy and significant enrichment in metals provide a direct clue to understanding the high turbulence of PNe around [WC]-type nuclei[19] and their higher C and N abundances[20]. IRAS 17514 provides the missing link between born-again events in low-mass stars such as V4334 Sgr (ref. [2]) and fully developed [WC]-nuclei, leaving open the possibility for our Sun itself, once it has become a PN[21], to experience a born-again event and conclude its life as a H-poor CSPN. The rapid evolution of HuBi 1 and its CSPN deserves close monitoring. The possible expansion of its inner shell, continuous dust production around the CSPN or its surface temperature increase can provide crucial insights into the formation of [WC] stars and deposition of energy and enriched material in the surrounding PNe.

## Methods

**Optical image of HuBi 1.** Optical images of HuBi 1 were obtained on 2 September 2008, using the ALhambra Faint Object Spectrograph and Camera (ALFOSC) at the 2.5 m Nordic Optical Telescope (NOT) of the Observatorio de El Roque de los Muchachos (ORM, La Palma, Spain). The EEV 2 K × 2 K CCD camera was used, providing a pixel scale of 0.184″ pix$^{-1}$ and a field of view (FoV) of 6.3′. Two 600 s exposures were obtained through narrow-band filters that isolate the [N II] $\lambda$6584 and H$\alpha$ $\lambda$6563 emission lines. These individual exposures were bias subtracted and flat-fielded using appropriate twilight sky frames, and then aligned and combined using standard iraf routines. The spatial resolution of the images, as derived from stars in the FoV, is 0.65″. The images were combined into the colour picture shown in Fig. 1a to highlight the different spatial locations of the H$\alpha$ recombination and low-ionization [N II] lines.

**Spatial profiles of selected emission lines of HuBi 1.** Long-slit optical spectra of HuBi 1 were obtained on 20 July 2014 using also ALFOSC at the 2.5 m NOT telescope. The 600 lines mm$^{-1}$ #7 and #14 grisms were used to acquire two 1,200 s exposures in the red and blue regions of the optical spectrum, respectively, covering the spectral range from 3,250 to 6,840 Å at a spectral resolution of 5.8 Å. The slit was placed at the central star along the east–west direction, that is, at a position angle (PA) of 90°. The spectro-photometric standard stars BD+33°2642 and BD+28°4211 were used for flux calibration. The seeing during the observations was 0.85″, as determined from the full-width at half-maximum (FWHM) of the continuum of field stars covered by the slit.

The two-dimensional spectra were used to extract spatial profiles of emission lines of interest along the long slit, that is, along the east–west direction across the central star. These spatial profiles were continuum subtracted using contiguous spectral regions free from emission lines. The emission line spatial profiles are 6 to 8 Å wide, whereas the redwards and bluewards contiguous background spatial profiles add together a width of 48 Å. Since the flux from the emission line is integrated and divided by the long-slit width and pixel scale, the resulting spatial profile represents the surface brightness of the nebula along this direction. Note that the [N II] $\lambda$6548 line is used for the [N II] spatial profile instead of the three times brighter [N II] $\lambda$6584 line because the latter is contaminated by bright stellar C II $\lambda\lambda$6578, 6582 emission lines.

These profiles are shown in Fig. 1b–d. Figure 1b shows the [N II] $\lambda$6548, H$\alpha$ $\lambda$6563 and He I $\lambda$5876 emission lines, the latter multiplied by 20. The spatial profiles of the H$\alpha$ and He I lines are similar and reveal the location of the outer shell. The spatial profile of the [N II] line peaks inside and reveals the location of the inner shell. The inner shell is shown in more detail in Figs. 1c and d. Figure 1d reveals that the spatial profile of the He II $\lambda$4686 line extends outside that of the [N II] $\lambda$6548 line, whereas the H$\alpha$ inner shell synthetic profile peaks between those of He II and [N II]. This synthetic inner shell H$\alpha$ spatial profile was obtained after subtracting a two-Gaussian model of the H$\alpha$ emission of the outer shell from the observed H$\alpha$ spatial profile in Fig. 1b.

**Age and morpho-kinematic modelling of the outer shell of HuBi 1.** Long-slit high-resolution spectra of HuBi 1 were obtained with the Manchester Echelle Spectrograph (MES) attached to the 2.1 m telescope of the OAN-SPM Observatory. Four 1,800 s spectra were obtained on 14 and 15 August 2015 with the slit oriented east–west (PA = 90°), and three 1,800 s spectra on 5 May 2018 with the slit oriented north–south (PA = 0°). In both cases, the slit was placed across the CSPN and the detector was a 2 K × 2 K E2V CCD in a 2 × 2 on-chip binning, leading to a dispersion of 0.057 Å pix$^{-1}$ and a spatial scale of 0.35″ pix$^{-1}$. The slit length is 6′.5 and its width was set to 1″. A $\Delta\lambda$ = 90 Å bandwidth filter was used to isolate the 87th order covering the H$\alpha$ and [N II] $\lambda\lambda$6548,6584 emission lines. A ThAr arc lamp was used for wavelength calibration to an accuracy of 1 km s$^{-1}$. The spectral resolution is 12 km s$^{-1}$, as indicated by the FWHM of the ThAr arc lines. The seeing was 1.2″–1.5″ during the observations.

The spectra at each PA were combined into a single long-slit spectrum. The position–velocity (PV) maps of the H$\alpha$ emission line from the outer shell are shown in the Supplementary Fig. 1. The H$\alpha$ emission line in the PV map at PA 90° appears as a velocity ellipse, although the detailed distribution of the emission in this map, with faint emission at high velocity at the nebular centre, is not completely consistent with a spherical shell. Indeed, the open tilted line emission in the PV map at PA 0° is suggestive of an elongated open-ended structure slightly tilted with respect to the line of sight.

To reproduce the observed H$\alpha$ PV maps and image of HuBi 1, we used the three-dimensional morpho-kinematic code SHAPE[22]. A barrel-like structure with fainter polar protrusions tilted with respect to the line of sight has been adopted to reproduce the general morphologies of the H$\alpha$ PV maps and image. A satisfactory fit is achieved with a barrel-like structure with aspect ratio $\gtrsim$1.0 whose symmetry axis is tilted to the line of sight by ≈25°. Adopting a distance of 5.3 kpc (ref. [23]), the kinematical age of the outer shell of HuBi 1 is found to be ≈9,000 yr.

**Non-LTE model of IRAS 17514.** Archival Isaac Newton Telescope (INT) Intermediate-Dispersion Spectrograph (IDS) optical spectra of IRAS 17514 (July 1996) were analysed using the Potsdam Wolf–Rayet (PoWR) model atmosphere code. PoWR is a state-of-the-art non-LTE radiative transfer code that accounts for mass loss, line blanketing and wind clumping[24]. It can be applied to a wide range of hot stars of arbitrary metallicities[25,26] with different luminosity $L$, stellar temperature $T_\star$, surface gravity $g_\star$ and mass-loss rate $\dot{M}$.

Initial stellar parameters[7] were refined on the basis of improved atomic data and line-blanket models including complex model atoms for H, He, C, N, O, Ne, Si and the iron group elements Sc, Ti, V, Cr, Mn, Fe, Co and Ni. A temperature of 38,000 ± 2,000 K is determined from the observed relative line strengths of C II $\lambda\lambda$4266.9,4267.9, C III $\lambda$5695.9 and C IV $\lambda\lambda$5801.3,5812.0, and those of Si III $\lambda\lambda$4552.6,4567.8,4574.8 and Si IV $\lambda\lambda$4088.8 4116.1. For a temperature of 36,000 K, the C III and C IV lines become much weaker in the model than in the observation, and the predicted Si III to Si IV line ratio becomes higher than observed. On the other hand, for a temperature of 40,000 K, the C III, C IV and Si IV lines in the model become too strong, whereas the C II and Si III lines appear too weak. In this best-fit model, shown in Supplementary Fig. 2, the luminosity log($L/L_\odot$) is 3.8 ± 0.3, the extinction $E_{B-V}$ 1.50 ± 0.05 mag, the stellar radius 1.8 $R_\odot$, the terminal wind velocity $v_\infty$ 360 ± 30 km s$^{-1}$, and the mass-loss rate ≈ 8 × 10$^{-7}$ $M_\odot$ yr$^{-1}$. The chemical abundances by mass fraction are 0.01–0.05 for hydrogen, 0.33 ± 0.10 for helium and 0.5 ± 0.1 for carbon, whereas rough estimates of 0.01 for nitrogen, 0.1 for oxygen, 0.04 for neon and 0.01 for silicon are obtained. Solar abundances of 1.4 × 10$^{-3}$ were adopted for iron.

**H I and He II ionizing flux.** The H I and He II ionizing flux can be derived from the intrinsic luminosity of the H$\alpha$ $\lambda$6563 and He II $\lambda$4686 emission lines using the relations:

$$Q(\mathrm{H\ I}) = L_{\mathrm{H}\alpha} / [j(\mathrm{H}\alpha) / \alpha_{\mathrm{B}}(\mathrm{H\ I})]$$
$$Q(\mathrm{He\ II}) = L_{\mathrm{He\ II}\,\lambda4686} / [j(\mathrm{He\ II}\,\lambda4686) / \alpha_{\mathrm{B}}(\mathrm{He\ II})]$$

assuming case B recombination and $T_e$ = 10,000 K in the low density case for the emission $j$ and recombination $\alpha$ coefficients. Assuming that the inner and outer shells are spherical and that the surface brightness profiles of the H$\alpha$ and He II $\lambda$4686 emission lines can be represented by those extracted along the east–west direction presented in Fig. 1b,d, the total flux corrected for reddening of these lines are 2.0 × 10$^{-12}$ and > 1.8 × 10$^{-14}$ erg cm$^{-2}$ s$^{-1}$, respectively. For the reddening correction, the extinction correction derived for the outer shell from the H$\alpha$ to H$\beta$ line ratio ($c$(H$\beta$) = 1.1) was applied. Since the extinction towards the inner shell might be larger, as suggested by an H$\alpha$/H$\beta$ line ratio larger than that of the outer shell, although based on an uncertain estimate of the H$\beta$ and H$\alpha$ fluxes of the inner shell, the He II flux of this shell should be regarded as a lower limit.

By adopting a distance to HuBi 1 of 5.3 kpc (ref. [23]), the H$\alpha$ and He II $\lambda$4686 Å fluxes imply luminosities of $L_{\mathrm{H}\alpha}$ = 7.0 × 10$^{33}$ erg s$^{-1}$ and $L_{\mathrm{He\ II}\,\lambda4686}$ ≥ 6.2 × 10$^{31}$ erg s$^{-1}$. The corresponding H I and He II ionizing photon fluxes are log$Q$(H I) = 45.7 and log$Q$(He II) ≥ 43.8, respectively. These ionizing fluxes can be compared to the output predicted by our non-LTE best-fit model to the spectrum of the CSPN. For the 1996 spectrum of the CSPN, this model predicts log$Q$(He II) = 34.3, much smaller than the value derived from the observed He II lines. This same model predicts log$Q$(H I) = 48, but the 2017 spectrum suggests that the H I ionizing flux has declined at least 4 orders of magnitude to log$Q$(H I) ≈ 44, also below the observed H I ionizing flux.

**Spectro-photometric evolution of IRAS 17514.** May 1991[4], July 1996 INT IDS, and July 2014 and May 2017 NOT ALFOSC optical spectra have been used, in conjunction with the original March 1989 *BVR* photometric data[3] and January 1971 USNO B-1 Catalog *BR* magnitudes[27], to investigate the spectro-photometric time evolution of IRAS 17514. The different spectra and photometric magnitudes are plotted in Fig. 2b. The observed flux in each spectra has been corrected from the seeing and slit-width, although this correction is small, of a few per cent. These spectra have also been used to fit a stellar continuum and determine the *BVR* magnitudes of the central star at each epoch. The time evolution of the flux of the star at different photometric bands is plotted in Fig. 2a.

**Spectral models of the inner and outer shells of HuBi 1.** The NOT ALFOSC two-dimensional spectra were also used to extract one-dimensional spectra of the inner and outer shells of HuBi 1 (Supplementary Fig. 3), using the apertures shown in Fig. 1b–d. A region of radius 0.7″ at the location of the central star was excluded to excise its emission from the spectrum of the inner shell.

The outer shell is dominated by H I and He I recombination lines, with much fainter [N II] $\lambda\lambda$6548,6584 and [S II] $\lambda\lambda$6716,6731, and no [O II] $\lambda$3727 or [O III] $\lambda\lambda$4959,5007 emission lines. The density-sensitive [S II] $\lambda\lambda$6716,6731 doublet has been used to derive an electronic density ≈200 cm$^{-3}$. At the distance of HuBi 1 and adopting a volume filling factor of 0.3 (ref. [23]), this density implies an ionized mass of 0.08 $M_\odot$, which is a reasonable value for a PN. The code MAPPINGS V 5.1.13 (ref. [28]) was used to explore the evolution of the intensity of various emission lines in a freely cooling gas. Supplementary Figure 4 shows the time evolution of the electronic temperature, ionization fraction of hydrogen, and emissivity of several emission lines for a spherical photoionized cloud of gas once the ionizing source is switched off and the gas is allowed to cool freely. The abundances have been assumed to be solar and the electron temperature to be 10,000 K. The electron density in the model is 200 cm$^{-3}$, as derived from the density-sensitive [S II] $\lambda\lambda$6717,6731 doublet line ratio. As time goes by, $O^{++}$, the most efficient coolant, is the first ion to fully recombine, followed by $O^+$, and then by $N^+$ and $S^+$. It takes longer for $He^+$ to recombine, whereas a significant fraction of hydrogen will remain ionized for a much longer period of time. The outer shell of HuBi 1 is found to be at a stage when the emissivities of the [N II] and [S II] emission lines are much higher than that of [O II]. In Supplementary Fig. 4, this occurs between 90 and 220 years after the central source is switched off, but we note that, whereas the overall behaviour of the gas remains the same, independently of the gas density (but for cases of extremely high metallicities), the time estimate may vary significantly depending on the metallicity of the gas and its density. The mild axisymmetry of the outer shell of HuBi 1 (see the description of the morpho-kinematical model) is not expected to affect significantly the main results presented here. Furthermore, these effects are certainly mitigated by the particular orientation of the long slit, mostly orthogonal to the outer shell symmetry axis.

As for the inner shell, the brightest emission lines in its spectrum are those of [N II]. Fainter emission is detected in the forbidden lines of [O I], [O II], [O III], [N I] and [S II], as well as in the recombination emission lines of H I and He I, and the notable detection of the He II $\lambda$4686 emission line. The presence of high ionization lines in the inner shell, together with its intricate profile structure, can be attributed to shocks, as the central source is no longer capable of appreciably ionizing the gas and producing $He^{++}$. To explore this possibility, we also used MAPPINGS to evaluate a shock expanding through a fully ionized ($H^+$/H = 1, $He^+$/He = 1) medium with solar abundances and a pre-shock density 200 cm$^{-3}$. The magnetic field was assumed to have a low value, $B_0$ = 0–1 μG. Shocks with velocities above 50 km s$^{-1}$ are required to produce [O III] emission, and above 70 km s$^{-1}$ to produce the observed value of the He II/H$\beta$ line ratio. Much higher shock velocities, above 100 km s$^{-1}$, can be firmly rejected as they imply line ratios very different from the ones observed. The emission structure behind a 70 km s$^{-1}$ shock is qualitatively consistent with that observed in the inner shell of HuBi 1, with the He II emission peaking outside at the shock region and [N II] and [O III] peaking inside in the post-shock cooling region.

**Low-mass very late thermal pulse models.** The evolved PN around IRAS 17514 and the strongly H-deficient composition of its stellar wind suggest a very late thermal pulse (VLTP) origin. In addition, the slow evolution of the central star implies a low-mass star. To test these assumptions, we computed several evolution sequences of VLTP events in low-mass stars using LPCODE, La Plata stellar evolution code. LPCODE is a one-dimensional stellar evolution code widely used for the computation of full evolutionary sequences from the zero age main sequence to the WD stage[29]. The last version of LPCODE has been carefully calibrated at different evolutionary stages to reproduce several AGB and post-AGB observables[30]. LPCODE has been successfully used to compute the evolution of post-AGB stars[30] and the formation of H-deficient stars through late helium flashes[31].

To create models of [WC] stars, we adopted some low-mass AGB models previously computed[30] and adjusted the stellar winds during the last stage of the AGB evolution to ensure that they left the AGB at the right time for a VLTP to take place in the post-AGB evolution of the sequence. The models correspond to initial masses 0.8 $M_\odot$ and 0.9 $M_\odot$ ($Z=0.001$) and 1 $M_\odot$, 1.1 $M_\odot$ and 1.25 $M_\odot$ ($Z=0.01$). The evolution of these sequences in the HR diagram is shown in the left panels of Supplementary Fig. 5, together with our luminosity and temperature determinations for IRAS 17514. The location of IRAS 17514 is consistent with a post-VLTP stage in all sequences. The surface abundances predicted for these VLTP models are shown in Supplementary Table 1, together with our determinations for the surface abundances of IRAS 17514. The qualitative agreement between the abundances measured in IRAS 17514 and the predictions of VLTP computations is remarkable, supporting a VLTP event in IRAS 17514.

These models should also reproduce the time behaviour of IRAS 17514. For this purpose, we show in the right panels of Supplementary Fig. 5 the time evolution of $T_{\rm eff}$ from the departure from the AGB ($\log T_{\rm eff}<3.7$) to the beginning of the WD phase ($\log T_{\rm eff}\sim 5$) and through the VLTP event (chosen as $t=0$). The low density and morphological appearance of HuBi 1 suggest it is an evolved PN, which is further supported by its kinematical age ≈9,000 yr. On the other hand, the outer nebula is recombining, indicating that the ionizing source faded 90–220 years ago, whereas spectroscopic observations of IRAS 17514 show that its temperature has stayed almost constant at $T_\star \simeq 38{,}000$ K for at least two decades.

The 0.8 $M_\odot$ and 0.9 $M_\odot$ sequences take ≈400,000 and ≈60,000 yr, respectively, between the departure from the AGB and the VLTP event, which is inconsistent with the estimated age of HuBi 1 (and even with the accepted visibility lifetime of PNe, ≈20,000 yr). Consequently, the evolution before the VLTP event can be used to reject very low-mass VLTP events. On the contrary, the time between the departure from the AGB and the point of maximum $T_{\rm eff}$ of the 1.0 $M_\odot$, 1.1 $M_\odot$ and 1.25 $M_\odot$ sequences is still below the accepted visibility lifetimes of PNe.

After the VLTP event, the 1.25 $M_\odot$ sequence stays as a born-again AGB giant for about 100 yr, then it reheats to 38,000 K, makes a double loop, crosses $T_{\rm eff}$ at 38,000 K again, stays as a giant for ≈150 years, and about 700 years after the star reheats back to 38,000 K. This sequence stays within the $T_{\rm eff}\simeq 36{,}000$–$40{,}000$ K range for only 1, 7 and 5 years in each crossing, respectively, and thus it does not reproduce the observed spectral behaviour of IRAS 17514 between 1989 and 2017. As for the 1.0 $M_\odot$ sequence, it is able to describe the behaviour of IRAS 17514 in this period of time, as well as the existence of an old evolved PN, but the time lapse between the departure from the AGB and the VLTP event for our 1.0 $M_\odot$ sequence cannot be shortened below ≃22,000 yr, resulting in a disagreement of a factor of two with the inferred kinematical age of the PN. Therefore, the VLTP evolution can be used to reject the 1.0 $M_\odot$ and 1.25 $M_\odot$ sequences, with the 1.1 $M_\odot$ sequence being the only one capable of reproducing accurately the time behaviour of IRAS 17514 and its nebula.

As shown in Fig. 3, the 1.1 $M_\odot$ sequence departs from the AGB about 12,000 yr before the occurrence of the VLTP event, in reasonable agreement with the kinematical age of HuBi 1. We note, however, that the post-VLTP evolution depends on the details of the mass removed by the stellar winds during the return to the AGB as a H-deficient giant (that is, the born-again AGB phase), which is very uncertain. Observations of bona fide VLTP events (V605 Aql, V4334 Sgr) indicate very high mass-loss rates, in the range $10^{-3}$–$10^{-5}$ $M_\odot$ yr$^{-1}$ (refs [2,32]), once the star becomes a cold AGB giant[1] ($\log T_{\rm eff}<3.8$). Consequently, we performed simulations of the post-VLTP evolution of our 1.1 $M_\odot$ sequence under different assumptions for the mass removed at $\log T_{\rm eff}<3.8$ during this phase. Supplementary Figure 6 shows the details of such simulations. In particular, a mean mass-loss rate of $7.6\times10^{-5}$ $M_\odot$ yr$^{-1}$, that is, within the observed range in other born-again events, allows us to reproduce the observed behaviour of IRAS 17514 between 1989 and 2017. The mass of the post-AGB star before the VLTP event is 0.551 $M_\odot$ and the total mass ejected amounts to $8\times10^{-4}$ $M_\odot$.

The time evolution of this sequence is shown in Fig. 3. This sequence matches most observed properties of HuBi 1 and its central star. It explains the existence of an old PN with kinematical age ≈9,000 yr, and the almost constant temperature $T_\star = 38{,}000\pm2{,}000$ K of the CSPN in the period of time between 1996 and 2014, its chemical enrichment and its stellar luminosity $\log(L/L_\odot)=3.75\pm0.3$.

**Code availability.** CLOUDY, MAPPINGS and SHAPE can be freely downloaded from https://www.nublado.org, https://mappings.anu.edu.au/code and http://www.astrosen.unam.mx/shape/index.html, respectively. The LPCODE and PoWR codes used in this paper are similarly available under request from M.M.M.B. and H.T., respectively. Note that LPCODE is not suitably written for public use.

**Data availability.** The data that support the plots within this paper and other findings of this study are available from the corresponding author upon reasonable request.

Received: 1 April 2018; Accepted: 9 July 2018;
Published online: 06 August 2018

## References

1. Duerbeck, H. W. et al. The rise and fall of V4334 Sagittarii (Sakurai's object). *Astron. J.* **119**, 2360–2475 (2000).
2. Hajduk, M. et al. The real-time stellar evolution of Sakurai's object. *Science* **308**, 231–233 (2005).
3. Hu, J. Y. & Bibo, E. A. Discovery of a new cool WR star in a low excitation planetary nebula. *Astron. Astrophys.* **234**, 435–438 (1990).
4. Pollacco, D. L. & Hill, P. W. The planetary nebula surrounding the WC 11 star IRAS 17514–1555. *Mon. Not. R. Astron. Soc.* **267**, 692–696 (1994).
5. Hamann, W.-R. in *Hydrogen Deficient Stars* Vol. 96 (eds Jeffery, C. S. & Heber, U.) 127 (Astronomical Society of the Pacific, San Francisco, 1996).
6. Peña, M. The low excitation planetary nebulae HuDo 1 and HuBi 1 and their [WC10] central stars. *Rev. Mex. Astron. Astr.* **41**, 423–433 (2005).
7. Leuenhagen, U. & Hamann, W.-R. Spectral analyses of late-type [WC] central stars of planetary nebulae: more empirical constraints for their evolutionary status. *Astron. Astrophys.* **330**, 265–276 (1998).
8. Corradi, R. L. M., Schönberner, D., Steffen, M. & Perinotto, M. Ionized haloes in planetary nebulae: new discoveries, literature compilation and basic statistical properties. *Mon. Not. R. Astron. Soc.* **340**, 417–446 (2003).
9. Draine, B. T. & McKee, C. F. Theory of interstellar shocks. *Annu. Rev. Astron. Astr.* **31**, 373–432 (1993).
10. Perea-Calderón, J. V., García-Hernández, D. A., García-Lario, P., Szczerba, R. & Bobrowsky, M. The mixed chemistry phenomenon in Galactic Bulge PNe. *Astron. Astrophys.* **495**, L5–L8 (2009).
11. Naito, H. et al. Five-year optical and near-infrared observations of the extremely slow nova V1280 Scorpii. *Astron. Astrophys.* **543**, A86 (2012).
12. Clayton, G. C. The R Coronae Borealis stars. *Publ. Astron. Soc. Pac.* **108**, 225–241 (1996).
13. Williams, P. M. Dust formation around WC stars. *Proc. IAU* **163**, 335 (1995).
14. Williams, P. M. Eclipses and dust formation by WC9 type Wolf–Rayet stars. *Mon. Not. R. Astron. Soc.* **445**, 1253–1260 (2014).
15. Acker, A. & Neiner, C. Quantitative classification of WR nuclei of planetary nebulae. *Astron. Astrophys.* **403**, 659–673 (2003).
16. Blöcker, T. Evolution on the AGB and beyond: on the formation of H-deficient post-AGB stars. *Astrophys. Space Sci.* **275**, 1–14 (2001).
17. Schönberner, D. Asymptotic giant branch evolution with steady mass loss. *Astron. Astrophys.* **79**, 108–114 (1979).
18. Zijlstra, A. A. The infrared [WC] stars. *Astrophys. Space Sci.* **275**, 79–90 (2001).
19. Acker, A., Gesicki, K., Grosdidier, Y. & Durand, S. Turbulent planetary nebulae around [WC]-type stars. *Astron. Astrophys.* **384**, 620–628 (2002).
20. García-Rojas, J. et al. Analysis of chemical abundances in planetary nebulae with [WC] central stars. II. Chemical abundances and the abundance discrepancy factor. *Astron. Astrophys.* **558**, A122 (2013).
21. Gesicki, K., Zijlstra, A. A. & Miller Bertolami, M. M. The mysterious age invariance of the planetary nebula luminosity function bright cut-off. *Nat. Astron.* **2**, 580–584 (2018).
22. Steffen, W. et al. Shape: a 3D modeling tool for astrophysics. *IEEE Trans. Vis. Comput. Graphics* **17**, 454–465 (2011).
23. Frew, D. J., Parker, Q. A., & Bojičić, I. S. The Hα surface brightness-radius relation: a robust statistical distance indicator for planetary nebulae. *Mon. Not. R. Astron. Soc.* **455**, 1459–1488 (2016).
24. Hamann, W.-R. & Gräfener, G. Grids of model spectra for WN stars, ready for use. *Astron. Astrophys.* **427**, 697–704 (2004).
25. Hainich, R. et al. Wolf-Rayet stars in the Small Magellanic Cloud. I. Analysis of the single WN stars. *Astron. Astrophys.* **581**, A21 (2015).
26. Reindl, N. et al. The rapid evolution of the exciting star of the Stingray nebula. *Astron. Astrophys.* **565**, A40 (2014).
27. Monet, D. G. et al. The USNO-B Catalog. *Astron. J.* **125**, 984–993 (2003).
28. Sutherland, R. S. & Dopita, M. A. Effects of preionization in radiative shocks. I. Self-consistent models. *Astrophys. J. Suppl. S.* **229**, 34 (2017).
29. Althaus, L. G. et al. The formation and evolution of hydrogen-deficient post-AGB white dwarfs: the emerging chemical profile and the expectations for the PG 1159-DB-DQ evolutionary connection. *Astron. Astrophys.* **435**, 631–648 (2005).
30. Miller Bertolami, M. M. New models for the evolution of post-asymptotic giant branch stars and central stars of planetary nebulae. *Astron. Astrophys.* **588**, A25 (2016).
31. Battich, T., Miller Bertolami, M. M., Córsico, A. H. & Althaus, L. G. Pulsational instabilities driven by the ∈ mechanism in hot pre-horizontal branch stars I. The hot-flasher scenario. *Astron. Astrophys.* **614**, A136 (2018).
32. Clayton, G. C. et al. Evolution of the 1919 ejecta of V605 Aquilae. *Astrophys. J.* **771**, 130 (2013).

## Acknowledgements
Some of the data presented in this article were obtained with ALFOSC, which is provided by the Instituto de Astrofísica de Andalucía (IAA) under a joint agreement with the University of Copenhagen and NOTSA. The Nordic Optical telescope (NOT) is installed in the Spanish Observatorio del Roque de los Muchachos of the Instituto de Astrofísica de Canarias, in the island of La Palma (Spain). This article is also based on observations carried out at the Observatorio Astronómico Nacional on the Sierra San Pedro Mártir (OAN SPM), Baja California, Mexico. We thank the daytime and night support staff at the OAN SPM for facilitating and helping obtain our observations. A.A. and C.M. acknowledge support through the CONACyT project CONACyT-CB2015-254132. G.R.-L. acknowledges support from Universidad de Guadalajara, Fundación Marcos Moshinsky, ProMoFID2018 and CONACyT (grant A1-S-12258). L.S. acknowledges support from PAPIIT grant IA-101316 (Mexico). L.F.M. is supported by Ministerio de Economía, Industria y Competitividad (Spain) grants AYA2014-57369-C3-3 and AYA2017-84390-C2-1-R (cofunded by FEDER funds). M.A.G. acknowledges support of the grant AYA 2014-57280-P, cofunded with FEDER funds. M.M.M.B. is partially supported through ANPCyT grant PICT-2016-0053 and MinCyT-DAAD bilateral cooperation program through grant DA/16/07. S.A.Z. was supported by the ITE-UNAM agreement 1500-479-3-V-04.

## Author contributions
M.A.G. planned the research project, programmed the observations, wrote the main body of the manuscript, and organized the writing of some subsections. A.A. performed the MAPPINGS simulations, C.M. the CLOUDY ones, and both devised the excitation nature of the inner and outer shells. C.K. estimated the ionizing flux necessary for the inner and outer shells. G.R.-L. reduced the imaging data and contributed to the analysis of the time evolution of the central star. H.T. analysed the spectrum of the central star using PoWR to determine its stellar parameters and abundances. L.S. and G.R.-L. obtained and reduced the high-dispersion spectroscopic observations, and together with L.F.M. and S.A.Z. analysed them using SHAPE. M.M.M.B. devised the post-AGB evolutionary scenario and computed the LPCODE VLTP evolutionary sequences. X.F. reduced the spectroscopic data and carried out the analysis of one-dimensional spectra and spatial profiles of emission lines. All authors contributed to the discussion of the different sections of this work.

## Competing interests
The authors declare no competing interests.

## Additional information
**Supplementary information** is available for this paper at https://doi.org/10.1038/s41550-018-0551-8.

**Reprints and permissions information** is available at www.nature.com/reprints.

**Correspondence and requests for materials** should be addressed to M.A.G.